PAPER

Check for updates

Strengthening biofilms with selective metal ions

Kiera J. Croland [ID] [a] and R. Kōnane Bay [ID] *[ab]

Biofilms are structured microbial communities consisting of bacteria embedded in a self-produced extracellular polymeric substance (EPS) that enables survival in diverse environments. The EPS can integrate materials from the surrounding environment, such as metal ions, which can provide additional mechanical protection to the embedded bacteria from environmental stressors. While previous studies demonstrated that metal ions impact the erosion behavior of biofilms, key quantitative properties, such as failure strain, remain largely undocumented due to difficulties in handling these viscoelastic and soft biomaterials. In this work, we introduce a technique to characterize the impact of metal ions on the uniaxial stress–strain response of bulk bacterial biofilms. Through applying this method to *Bacillus subtilis* pellicles, we demonstrate that exposure to selective metal ions increases both the low strain elastic modulus and maximum stress, while decreasing failure strain. These effects are consistent with ion-mediated EPS crosslinking and are reversible through the introduction of a strong chelating agent, while variations in pH alone have a negligible impact on measured mechanical properties. We compare our results to previous biofilm erosion studies and provide insights into how metal ion interactions can alter the mechanical behavior of biofilms, which will aid in future biofilm mitigation strategies for biofouling or healthcare applications.

1. Introduction

Biofilm-forming bacteria increase their resilience to the surrounding environment by aggregating together and encasing themselves in an extracellular polymeric substance (EPS). Biofilms are complex structures that readily colonize diverse surfaces, including human tissue,[1,2] medical devices,[3,4] and water distribution systems.[5,6] The protective EPS provides constituent bacteria with structural integrity, surface adhesion, and protection from antimicrobial agents.[7] As a result, biofilms pose significant challenges across many industries.[5] In clinical settings, biofilm infections resist conventional antibiotic therapy and often require surgical intervention for complete removal.[2] Biofilms that form on equipment surfaces in industrial settings, such as tanks and pipes, similarly require costly interventions through physical removal or equipment replacement.[5,6] Despite these challenges, biofilms can be engineered to offer significant benefits. In wastewater treatment facilities, biofilms serve as bioreactors that efficiently degrade organic pollutants and remove contaminants from effluent streams.[8] Additionally, biofilm properties can be exploited in engineered living materials (ELMs)[9,10] to create stimuli-responsive intelligent systems. Across all applications, mechanical properties fundamentally govern biofilm behavior, yet characterization of these fragile biological materials remains technically challenging.[11,12]

Current approaches to biofilm mechanical characterization often yield results that are difficult to compare across systems due to a lack of standardization.[11,12] Many mechanical testing methods for biofilms disrupt the native biofilm architecture during sample preparation and mounting (*e.g.*, shear rheometry),[1,13–19] do not yield quantitative mechanical parameters (*e.g.*, no decipherable modulus,[20] relative detachment values,[13–15] and stability[21]), and do not capture responses under physiologically relevant conditions.[22–24] While microscale techniques (*e.g.*, microrheology[25] and AFM) preserve the local structure, they do not reflect bulk mechanical behavior, which is essential for understanding the macroscopic behavior of these inherently heterogenous structures. Furthermore, laboratory-grown biofilms often lack the complexity found in natural environments. *In situ* biofilms routinely incorporate external molecules or components from their surroundings into the EPS, altering material properties. Environmental factors, such as nutrient availability[21] and host conditions,[1] have been shown to influence the EPS composition and production. Therefore, it is critical to understand how environmental stimuli, such as the exposure to metal ions,[13,14] biopolymers,[15] or antibiotics,[15] impact biofilm mechanics.

Metal ion interactions with the EPS are of particular interest due to their prevalence on colonized surfaces. Metal ions are abundant in biological settings, such as within the human body

[a] Department of Chemical & Biological Engineering, University of Colorado Boulder, Boulder, USA. E-mail: konane.bay@colorado.edu

[b] Materials Science and Engineering Program, University of Colorado Boulder, Boulder, USA

(*e.g.*, blood and tissues) and on abiotic surfaces (*e.g.*, metal pipes and industrial processing tanks). Additionally, bacteria are able to deteriorate metals through microbially induced corrosion (MIC).[26] Although metal ions can exhibit toxicity to planktonic bacteria,[13,27] biofilms can actively incorporate ions into the EPS, leading to their long-term survival. Prior studies have demonstrated that treatment with metal ions can significantly influence biofilm mechanical properties, such as modulus (*via* shear rheology),[13,14,19,28] adhesion or failure behavior (*via* erosion assays),[13,14] and surface hydrophobicity.[29] However, standard shear rheology techniques for biofilms often require scraping colonies from solid substrates and loading them onto a rheometer, which disrupts the biofilm structure. Erosion studies preserve the biofilm structure but do not yield quantitative mechanical parameters.

In this work, we introduce a new approach to tensile testing bacterial biofilms. Our approach builds on existing rheological, erosion resistance, and tensile testing techniques by quantitatively capturing both high- and low-strain behavior in response to exogenous environmental signals. Tensile stresses are physiologically relevant to biofilms in flow environments, such as pipes or catheters, where shear flow can induce extensional (stretching) deformation of surface-attached biofilms. We employ the soil-dwelling, non-pathogenic bacterium *Bacillus subtilis* (*B. subtilis*) as our model organism due to its well-characterized genetic regulation of biofilm formation[30] and matrix composition,[31] robust biofilm formation capabilities,[32] and precedence in biofilm mechanics research.[13–15,17,20,22–24,33] *B. subtilis* is also ecologically and practically significant—it colonizes in the human gastrointestinal tract,[34] is used as a probiotic,[35] and forms root-associated biofilms that promote nutrient uptake.[36] Prior work has applied tensile testing to *B. subtilis* colonies on agar plates[20] as well as pellicles,[22,23] which are biofilms that grow at the air–liquid interface; however, these studies were limited by their ability to provide quantitative mechanical parameters and long experimental timelines, respectively. The method described here implements a custom-built cantilever-based instrument, The Uniaxial Tensile Tester for UltraThin films (TUTTUT), which has previously been used for tensile testing on synthetic polymer ultrathin films (<200 nm).[37–41] Critically, TUTTUT characterization preserves the native pellicle structure, enables the introduction of environmental cues at various points of biofilm development, and provides quantitative measurements of mechanical properties across the complete strain range in one test. Using this method, we find that *B. subtilis* pellicles display viscoelastic behavior, consistent with previous reports.[22,23] To investigate how environmental metal ion incorporation influences biofilm mechanical response, we characterized how the *B. subtilis* pellicle stress–strain response changes upon exposure to Fe^{3+}, Fe^{2+}, Cu^{2+}, Cu^+, Ca^{2+}, and Na^+. Our results suggest that certain metal ions can significantly impact low strain elastic modulus (E), maximum stress (σ_{max}), and failure strain (ε_f), providing quantitative insight into metal ion effects on biofilm mechanics and demonstrating the versatility of our TUTTUT system for studying the impact of diverse environments on the mechanical behavior of biofilms.

2. Results and discussion

Here, we modify TUTTUT to directly measure the uniaxial stress–strain response of *B. subtilis* pellicles (Fig. 1A). Prior to tensile testing biofilms, TUTTUT was used to characterize the stress–strain response of ultrathin polymer films (<200 nm).[37–41] TUTTUT leverages a liquid support bath to manipulate difficult-to-handle materials, making it well-suited for characterizing ultrasoft biofilms (*i.e.*, ~100 Pa–10 kPa[13–15,22,23]). TUTTUT is a cantilever-based method, in which force resolution can be tuned by adjusting the material and geometry of the cantilever, enabling precise force measurements across a wide modulus
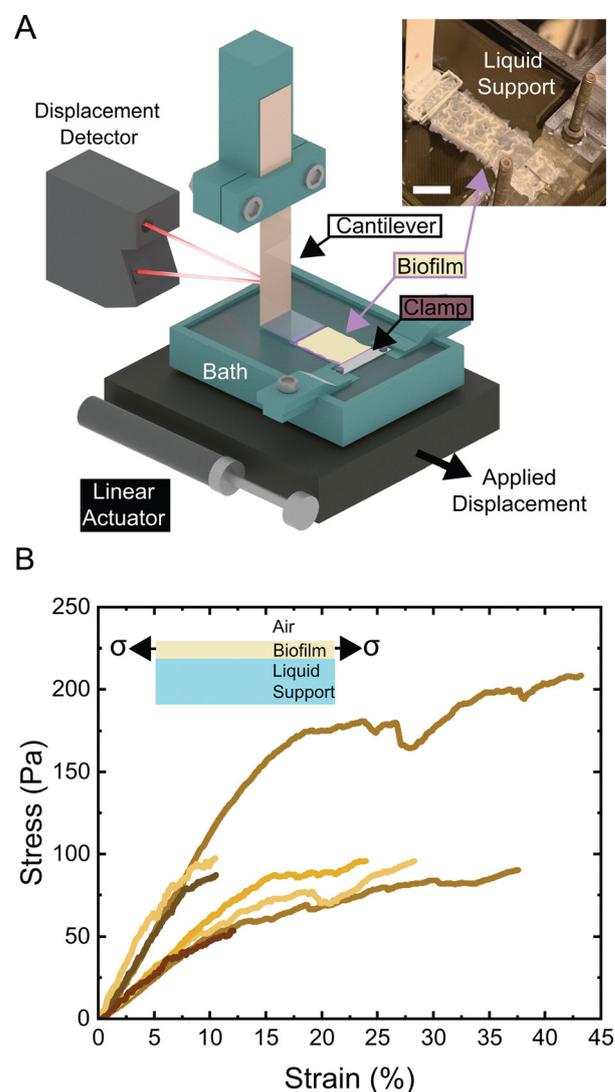

Fig. 1 TUTTUT measurements of the complete uniaxial stress–strain response of *B. subtilis* pellicles. (A) Diagram of the uniaxial tensile tester for ultrathin films (TUTTUT) showing a pellicle atop the liquid support bath, held between a rigid boundary (clamp) and a flexible cantilever. The inset (top right) shows a *B. subtilis* pellicle prior to tensile testing in TUTTUT (scale bar 1 cm). The pellicle is atop the liquid support bath, again, held between the cantilever and the clamp. (B) Stress–strain curves for all untreated *B. subtilis* pellicles measured (*n* = 7). The inset shows side view illustration of a pellicle being stretched on a liquid support.

range—from soft biofilms with elastic moduli in the Pa range to stiff polymer films in the GPa range. This makes TUTTUT broadly applicable to materials with widely varying mechanical properties. To the best of our knowledge, only one other research group has tested the tensile properties of pellicles.[22,23] Their approach, however, relies on growing the biofilm directly on the liquid surface within their instrument, resulting in natural adhesion onto the force sensors and instrument walls. While this approach preserves *in situ* biofilm growth, it constrains experimental throughput and parameter space, as evidenced by the authors' report of approximately 100 biofilms studied over five years.[22]

In this work, *B. subtilis* pellicles are grown outside of the liquid support bath in TUTTUT (Fig. 1A), allowing successive measurements without culture time restraints. We accomplish this by growing rectangular pellicles in 3D printed molds which generate two rectangular test samples from a connected media source (see the Experimental methods section and Fig. S1). To minimize clamping and end effects, samples were prepared with lengths greater than their widths (aspect ratios 1.85–3.86 (L/W), see the SI). Prior work on rectangular freestanding polymer thin films has shown that apparent geometry dependent differences in tensile response primarily arise from system compliance rather than intrinsic material behavior.[42] After growth, additional liquid media are added to the culture container to float the biofilms out of the molds (Movie S1 and Fig. S2). One biofilm is transferred to TUTTUT, and the other is harvested onto a glass slide for determining the biofilm thickness (see the Experimental methods section and Fig. S3). Because tensile testing and thickness measurements are performed on two separate pellicle strips, some variability between films could introduce error into the calculated stress. Films grown within the same culture container exhibited an average thickness difference of $10.6 \pm 8.88\%$ (Fig. S4). Additional sources of uncertainty may arise from surface wrinkling or trapped water during optical profilometry measurements of pellicles on glass slides. However, these effects were minimized through consistent handling and imaging conditions and are not expected to substantially alter the reported mechanical trends. After transferring the biofilm to the bath, the biofilm is attached to the bath and the cantilever (Fig. 1A). To perform tensile testing, a linear actuator stretches the biofilm at a constant strain rate (0.0026–0.0045 s^{-1}, previously used in *B. subtilis* tensile testing[22]) causing the cantilever to deflect. The cantilever is calibrated for force and displacement, and using biofilm geometry, we calculate stress and strain (see the Experimental methods section).

The stress–strain curves for untreated *B. subtilis* pellicles are shown in Fig. 1B. Similar to what has previously been observed,[22] there is an initial linear-elastic regime at low strains followed by nonlinear behavior. Low strain elastic modulus (E) was determined from the slope of the stress–strain curve between 0 and 5% strain (Fig. S5). To assess the influence of a potential toe region, linear fits were also performed excluding the initial 0.5% strain; however, consistent E trends were obtained in both analyses (see Table S1). In addition, E was also calculated from linear fits over the 0–10% strain range (Table S2). Because some

samples exhibited non-linear behavior beginning around 6% strain for some samples (see Fig. S5C), E values reported in the main text are based on the 0–5% strain region. Notably, two populations of E within the stress–strain curves appear to be present for untreated pellicles, despite being prepared and tested under the same conditions; however, we found no clear factors (*e.g.* sample history or handling) that could account for the variation. We determine the low strain elastic modulus, $E \sim 850 \pm 310$ Pa, the maximum stress, $\sigma_{max} \sim 120 \pm 62$ Pa, and the failure strain, $\varepsilon_f \sim 26 \pm 15\%$. E and σ_{max} are of the same order of magnitude as the literature values ($E \sim 200$–400 Pa and $\sigma_{max} \sim 50$–200 Pa).[22,23] In prior tensile studies, residual compressive stress is present due to pellicle growth in the testing apparatus.[22,23] Here, we release pellicles from their culture molds prior to loading, thereby relieving growth-induced compressive stresses and defining a relaxed reference state for tensile deformation. Variations between our results and previously reported values may be attributed to differences in sample age and thickness measurement protocols. In this study, samples were tested on day 3, whereas prior studies evaluated samples aged for 2 (ref. 22) or 4–7 (ref. 23) days. Moreover, the thickness was measured individually for each culture container using optical profilometry in the present work, while previous studies assumed a constant average thickness of 350 μm across all samples, as measured using a needle plunge technique and microscopy.[22–24] Furthermore, whereas previous researchers required five years to collect data on over 100 pellicles,[22] TUTTUT enabled the characterization of 82 pellicles within just 26 testing days, corresponding to an average throughput of approximately ~ 3.2 samples per day. We note that a small number of tensile tests were excluded from analysis due to pellicle slipping at the cantilever or clamp (12 samples) or due to experimental setup issues (15 samples). However, even with these exclusions, our throughput is still a substantial improvement in experimental efficiency compared to previous tensile testing methods.

Beyond increasing the throughput for measuring the mechanics of untreated pellicles, TUTTUT provides a platform to measure the influence of external environmental factors (*e.g.* free metal ions) on the mechanical properties of biofilms (Fig. 2). Here, we assess the impact of Cu^{2+} and Fe^{3+}, which are relevant to biofilms in copper and iron piping systems. We subsequently tested Fe^{2+} and Cu^+ to probe the impact of metal identity and ion valency. Additionally, we probe the influence of Ca^{2+} and Na^+, which are common free metal ions in water systems.[43,44] After three days of growth, pellicles were released from their molds and exposed to 50 mM metal ion solutions for one hour by replacing the culture media with metal-supplemented media, such that they are in a free-floating state (see the Experimental methods section and Fig. S2). The metal ion concentration and exposure time were selected to mirror previous studies employing rheology and erosion analyses to probe the influence of metal ion exposure on biofilm mechanics. Additionally, we calculated an estimated diffusion time of ~ 36 minutes, assuming the highest biofilm thickness (859 μm), lowest ion diffusivity (0.604×10^{-9} m^2 s^{-1} for Fe^{3+}),[45] and ratio of effective diffusivity through biofilms to aqueous diffusivity (0.56).[46] Treatment with 50 mM Fe^{3+} and Cu^{2+}
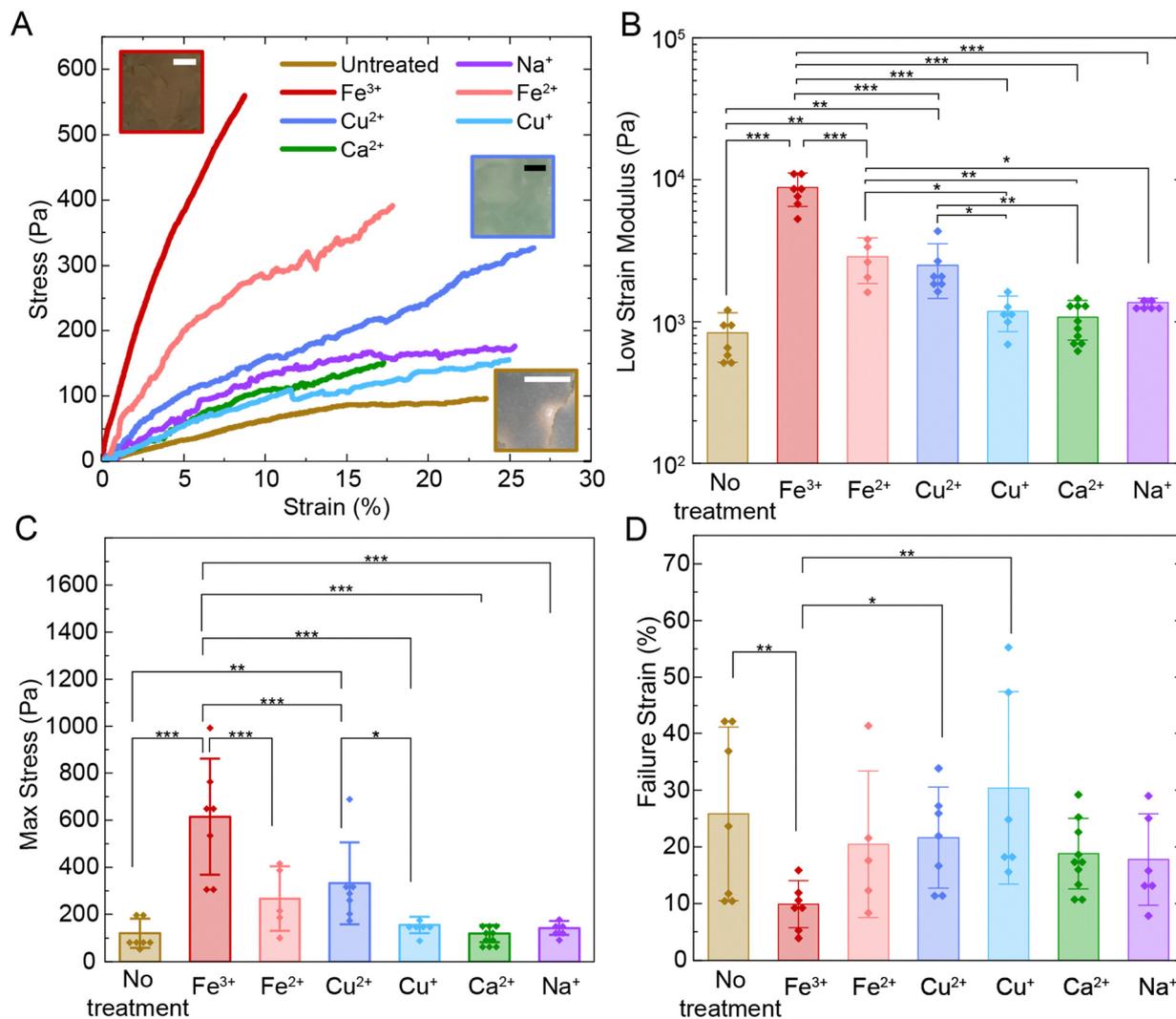
Fig. 2 Treatment with selected metal ions (Fe^{3+}, Fe^{2+}, Cu^{2+}, Cu^+, Ca^{2+}, and Na^+) impacts the stress–strain response of *B. subtilis* pellicles. (A) Individual representative stress–strain curves with representative images of treated (Fe^{3+} and Cu^{2+}) and untreated biofilms (scale bar 200 μm) and extracted average (B) low strain elastic modulus, (C) maximum stress, and (D) failure strain for untreated pellicles ($n = 7$) as well as those incubated in media supplemented with 50 mM $FeCl_3$ ($n = 7$), $FeCl_2$ ($n = 5$), $CuSO_4$ ($n = 7$), $CaCl_2$ ($n = 10$), $CuCl$ ($n = 6$), or $NaCl$ ($n = 6$) for one hour. Data are represented as mean $\pm$ standard deviation (SD). Statistical significance is determined using a one-way analysis of variance (ANOVA) with a Fisher's least significant difference (LSD) *post hoc* test. $p < 0.05$, $p < 0.01$, and $p < 0.001$ are indicated with an *, **, and ***, respectively. Data for this figure are included in the SI (FullData.xlsx).

resulted in a pellicle color change from off-white to rust and blue (Fig. 2A), respectively, indicating the absorption of these ions into the biofilm matrix. We observe no change in lateral dimension; however, we note a reduction in thickness compared to that of untreated biofilms for all metal ion treatments except Fe^{3+}-treated pellicles. This change in thickness is accounted for in stress calculations. For all metal ion treatments, we measure a stress–strain curve with a shape similar to that of the untreated biofilms (Fig. 2A). Metal ion treatment leads to an increase in E and σ_{max} as well as a decrease in ε_f compared to the untreated biofilms (Fig. 2B–D). To understand the impact of different metal ion treatments on biofilm mechanics, we compare E, σ_{max}, and ε_f.

Among pellicles treated with the trivalent ion, Fe^{3+} had the largest increase in the average E—an increase by an order of

magnitude—followed by Fe^{2+}-treated pellicles, which resulted in a >3-fold increase in E, and then Cu^{2+}-treated pellicles (~ 2.9-fold increase in E, Fig. 2B). Pellicles treated with other bivalent and monovalent ions exhibit a more moderate increase in E, although these changes are not statistically significant (Fig. 2B). It should be noted that Fe^{2+} and Cu^+ solutions likely underwent partial oxidation to Fe^{3+} and Cu^{2+}, respectively, as suggested by a slight color change in the surrounding media during testing. Thus, the mechanical responses observed for these samples may reflect contributions from both oxidation states rather than a single, well-defined ionic species. Researchers have observed similar increases in the storage modulus (G') for *Pseudomonas aeruginosa* (*P. aeruginosa*),[28] *Escherichia coli*,[19] and *B. subtilis* (B-1[13] and NCIB 3610[14]) colonies with the addition of trivalent metal cations. Increases in E have also

been observed in *P. aeruginosa* biofilms with Ca^{2+} exposure due to Ca^{2+}-mediated ionic crosslinking of alginate in the *P. aeruginosa* EPS.[47] The increase in E with Fe^{3+} and Cu^{2+} treatment seen in this work is consistent with previously reported changes in G' for ion-treated NCBI 3610 colonies;[14] however, while we observe a slight, although not significant, increase in E with Na^+ and Ca^{2+} treatment, previous measurements show a decrease or no change in G'.[13,14] This discrepancy may arise from differences in sample preparation or growth method, which are known to influence the measured mechanical properties of biofilms.[48] Here, tensile tests are performed on pellicle biofilms, whereas previous work implemented shear rheology and erosion assays on biofilm colonies grown on agar plates.

The increase in E is associated with nonspecific ionic crosslinking between EPS components and metal ions. In *B. subtilis*, positively charged metal cations interact with negatively charged functional groups on proteins (*e.g.*, carboxylic acid and aspartate), leading to increased crosslinking of the EPS.[26,49,50] Additionally, cryo-electron microscopy on the *B. subtilis* EPS component TasA has suggested that aspartate residues on TasA can coordinate metal cations.[51] Furthermore, erosion assays performed on metal ion-treated NCIB 3610 colonies, specifically those performed on mutants lacking key EPS components, demonstrated that enhanced biofilm attachment arises from interactions between the metal ions and the EPS, not specific to any particular EPS component.[14] This mechanism parallels that of metal-ion coordinated hydrogels, where reversible coordination between multivalent cations and polymer functional groups enhances mechanical properties, such as stiffness and toughness.[52] Biofilms are often compared to colloidal hydrogels, where the cells are the colloids and the EPS is the crosslinked gel.[49,53,54] Similar to the structural role that metal ion coordination plays in hydrogels, ion coordination in biofilms may reinforce the EPS through dynamic crosslinking interactions. Although Na^+ is monovalent and therefore unlikely to form crosslinks in the biofilm matrix, its addition is associated with a modest, though not statistically significant, increase in E. This effect may arise from nonspecific ionic screening that reduces electrostatic repulsion within the EPS and/or osmotic deswelling of the biofilm matrix.

In further support of our ionic crosslinking hypothesis, we observe a trend of decreasing ε_f with the addition of the metal ions (Fig. 2D). Although Fe^{3+} treated biofilms are the only group which displays a statistically significant decrease in ε_f from the untreated biofilms, a trend of decreasing ε_f with metal ion treatment is present. We propose that this decrease arises from an increase in network connectivity—specifically, higher crosslink density—which limits the ability of the biofilm to deform before failure. This interpretation aligns with findings from tensile tests on ionically crosslinked hydrogels, where increasing crosslink density, achieved through increased metal cation content, leads to a reduction in ε_f.[55] In further support of ion-mediated stabilization, previous work showed that supplementing *B. subtilis* NCIB 3610 cultures with Ca^{2+} limits biofilm dispersal by promoting structural stabilization,[56] suggesting that metal ion-induced stabilization may influence biofilm

persistence and failure. To our knowledge, this is the first quantification of ε_f in *B. subtilis* pellicles. We note that ε_f has been quantified for the surface of other biofilms using a microcantilever-based technique.[57]

Two failure modes were commonly observed during tensile testing: either failure initiated at pre-existing cracks introduced during removal from culture molds or new cracks or holes formed and propagated under tension. In most cases, failure occurred near the grip interface, typically within approximately 5 mm from the end of the film. While the presence of pre-existing cracks did not appear to significantly alter the ε_f, samples with pre-existing cracks tended to exhibit lower maximum stress values at failure (Table S3). However, definitive conclusions cannot be drawn due to a limited number of replicates.

The addition of metal ions results in an increase in σ_{max}, with Fe^{3+} producing the highest σ_{max}, followed by Cu^{2+}, Fe^{2+}, Cu^+, and then Na^+ (Fig. 2C). Similar trends are seen in yield stress, σ_y (see Fig. S6). We attribute these increases to ionic crosslinking; however, we note that the differences in σ_{max} between the untreated group and the Fe^{2+}, Cu^+, Na^+, and Ca^{2+} treated groups are not statistically significant. Because σ_{max} reflects the maximum stress a biofilm can sustain prior to failure, it is relevant for understanding biofilm resistance to extreme mechanical perturbations, such as high shear or disruptive forces.

Differences in σ_{max} values between metal ion treatments have several potential sources, including variations in the spatial distribution of the metal ions within the EPS or metal ion electronic structure. X-ray fluorescence (XRF) measurements from prior work support this idea, showing that Ca is distributed uniformly throughout the biofilm matrix, whereas Zn, Mn, and Fe are specifically enriched within biofilm wrinkles.[58] The spatial distribution of ionic crosslinks can influence mechanical behavior by creating regions of localized stress concentration that are more susceptible to crack initiation,[59] which can impact the measured σ_{max}. In addition to spatial effects, differences in metal identity may also contribute to the observed changes in all properties measured. For example, in alginate hydrogels crosslinked with metal ions, E follows the trend, $Fe^{3+} > Cu^{2+} > Ca^{2+}$, which is attributed to differences in ion charge, size, coordination number, and binding affinity. Trivalent ions, like Fe^{3+}, can coordinate with three carboxylic groups on alginate, forming more crosslinks and generating stiffer networks. Divalent ions such as Fe^{2+}, Cu^{2+} and Ca^{2+} typically coordinate with two groups, leading to more compliant structures.[60] We observe a similar trend in biofilms, where Fe^{3+} treatment induces the largest change in measured properties among all ions tested. The difference in E for Cu^{2+} and Ca^{2+} crosslinkers in alginate hydrogels was attributed to the affinity of each ion to binding alginate.[60] This could play a role in the differences in E observed in biofilms for divalent crosslinkers here: ions may have differing affinities for EPS polymers. Additionally, metal ions exhibit preferred coordination geometries based on their electronic configurations, but the specific binding environments presented by EPS components may constrain ions into less favorable geometries,[52] giving rise to metal identity-dependent mechanical properties.

To test our ionic crosslinking hypothesis, we introduced an additional wash step to remove metal ions from pellicles pre-treated with Fe^{3+}. Fe^{3+} was selected for this study because it caused the most pronounced mechanical differences from untreated biofilms. In this study, following treatment with 50 mM Fe^{3+}, pellicles were subjected to a secondary one hour wash step using LB–glycerol–manganese (LBGM) media or 25 mM ethylenediaminetetraacetic acid disodium salt (EDTA), a strong chelating agent. The LBGM media wash results in slight recovery of the stress–strain response (Fig. 3A) and moderate reduction of the rust color associated with Fe^{3+} treatment (Fig. 3A). These changes suggest limited removal of Fe^{3+} ions and partial disruption of the ionic crosslinks within the EPS using LBGM media. In contrast, the EDTA wash produces a more dramatic color change, indicating more effective removal of Fe^{3+} from the EPS (Fig. 3A). Mechanically, the EDTA wash resulted in pellicle stress–strain curves and mechanical property metrics (E, σ_{max}, or ε_f) that closely resembled those of EDTA-only controls (*i.e.*, pellicle treated with EDTA but no Fe^{3+}), indicating reversal of Fe^{3+} induced stiffening (Fig. 3B–D, refer to Fig. S7 for yield stress). The stronger impact of EDTA wash compared to that of the LBGM media wash is due to the high affinity of EDTA for metal ions,[61,62] allowing it to more effectively disrupt Fe^{3+}–EPS interactions. While color changes and EDTA reversibility support ionic participation, additional studies would be required to directly quantify metal content or map its spatial distribution within the EPS. Trends seen here agree with erosion studies on *B. subtilis* B-1 colonies, where an EDTA wash following Fe^{3+} treatment restored biofilm detachment to ∼100%.[13]

Notably, treatment with EDTA alone seemed to impact biofilm mechanics. While the Na^+ ions present in the EDTA solution could contribute to the observed changes, EDTA-specific interactions are also likely to play a role. In contrast
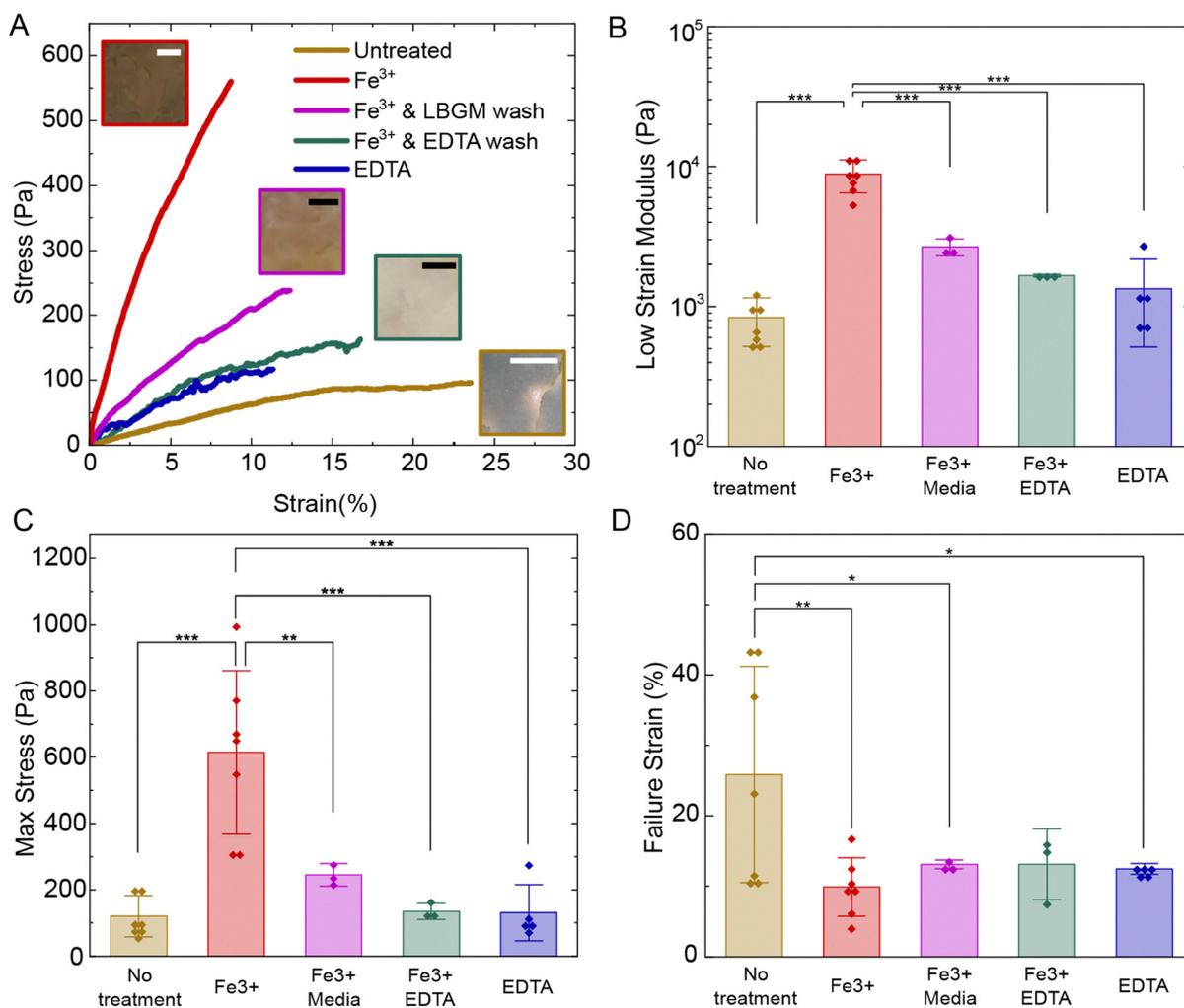

Fig. 3 Mechanical characterization of pellicles following Fe^{3+} treatment and subsequent wash steps. Here, pellicles are exposed to 50 mM Fe^{3+} for one hour followed by a wash with 25 mM EDTA or LBGM media. (A) Representative stress–strain curves and biofilm images (scale bar 200 μm) and comparison of average (B) low strain elastic modulus, (C) maximum stress, and (D) failure strain across treatment groups (untreated ($n = 7$), Fe^{3+} ($n = 7$), EDTA wash ($n = 3$), LBGM wash ($n = 3$), EDTA only (no Fe^{3+} pre-treatment, $n = 5$)). Data are represented as mean ± SD ($n \geq 3$). Statistical significance is determined using a one-way ANOVA with a Fisher's LSD *post hoc* test. $p < 0.05$, $p < 0.01$, and $p < 0.001$ are indicated with an *, **, and ***, respectively. Data for this figure are included in the SI (FullData.xlsx).
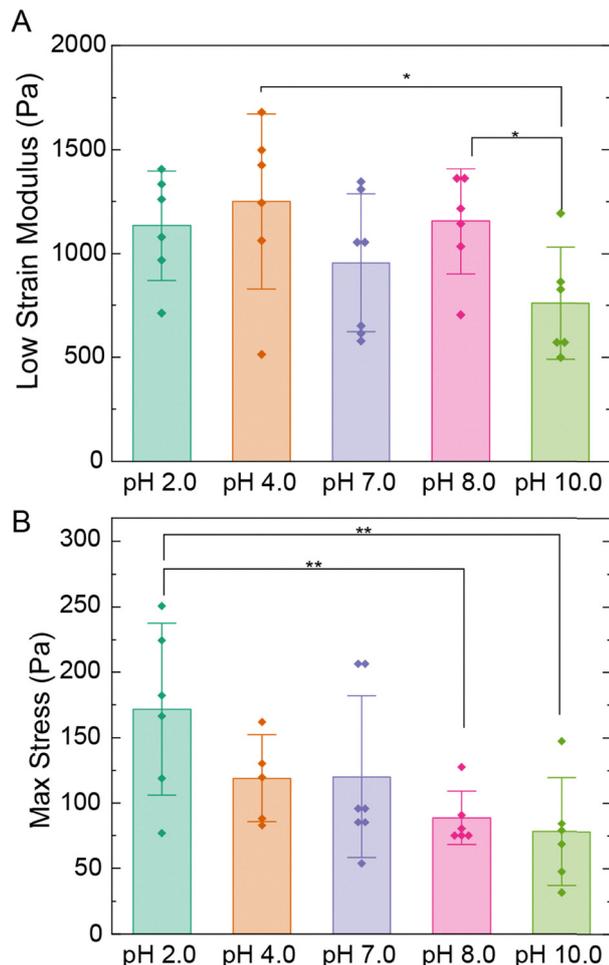
Fig. 4 Treatment with LBGM media adjusted to pH 2.0 (n = 5), 4.0 (n = 5), 8.0 (n = 6), and 10.0 (n = 6) results in small changes in (A) average low strain elastic modulus and (B) maximum stress for *B. subtilis* pellicles. See Fig. S9 for failure strain values and Table S3 for the pH of all treatment fluids used in this study. Data are represented as mean ± SD. Statistical significance is determined using a one-way ANOVA with a Fisher's LSD *post hoc* test. $p < 0.05$, $p < 0.01$, and $p < 0.001$ are indicated with an *, **, and ***, respectively. Data for this figure are included in the SI (FullData.xlsx).

to prior findings showing that EDTA compromises the structural integrity in biofilms formed by pathogenic bacteria,[63,64] we see a slight decrease in ε_f for the EDTA only treatment, potentially indicative of increased network connectivity. This mechanical response could be influenced by interactions between EDTA and extracellular DNA (eDNA) in the EPS[65] or pH effects.[58,66] Previous studies have suggested that EDTA may enhance single-stranded DNA binding to *B. subtilis* cells,[65] potentially introducing additional crosslinks within the biofilm matrix and contributing to the observed reduction in ε_f. Additionally, previous work has shown that TasA fibers exhibit polymorphism and undergo configurational changes or aggregation under acidic conditions.[58,66] This may result in biofilm matrix stiffening due to EDTA exposure and could impact stress–strain behavior.

Given the acidity of EDTA and that the addition of metal ions to LBGM media causes a reduction in pH (Table S4), we

next explored the impact of pH on the biofilm tensile response. Similar to our metal ion studies, we perform TUTTUT testing on pellicles exposed to LBGM media adjusted to pH 2.0, 4.0, 8.0, and 10.0 for one hour (Fig. 4 and Fig. S8 and S9). Treatment with pH adjusted media causes slight changes in measured mechanical properties for a few treatment groups, although much smaller than those caused by the metal ion solution with its corresponding pH. Thus, we attribute the increase in E and σ_{max} and the decrease in ε_f to the presence of metal ions as opposed to the pH change. However, LBGM media adjusted to pH 4.0, which is closest to the pH of 25 mM EDTA, result in a moderate increase in E and a decrease in ε_f, suggesting that pH may contribute to the effects observed with EDTA treatment.

3. Conclusions

We introduce a method, TUTTUT, to directly measure the uniaxial stress–strain relationship of bacterial biofilms. Using TUTTUT, we find that the E, σ_{max}, and ε_f of *B. subtilis* pellicles are impacted by the absorption of the metal ions Fe^{3+}, Fe^{2+}, Cu^{2+}, Cu^+, Na^+, and Ca^{2+} into the biofilm matrix. pH is found to have a minimal influence on the observed changes in mechanical properties. Additionally, the mechanical properties of untreated pellicles can be partially recovered from Fe^{3+} pretreated pellicles through the introduction of a chelating agent, EDTA. The role of metal ions in controlling biofilm mechanics highlights the importance of considering the ionic environment when developing strategies for biofilm removal or control. The presence of strongly bound metal ions, such as Fe^{3+}, may confer increased mechanical stability, making biofilms more resistant to mechanical removal. Effective biofilm mitigation strategies may therefore require the identification and targeted removal of ions from the EPS. Furthermore, these results are relevant to a wide range of applications in which biofilms interact with materials—such as medical devices, water infrastructure, and industrial surfaces—where local ion availability may significantly influence the biofilm structure, persistence, and response to treatment.

4. Experimental methods

4.1 Bacterial culture

Liquid cultures of *B. subtilis* NCIB 3610 were generated by inoculating 2% w/v LB broth (Lennox) with a piece of frozen bacterial glycerol stock, incubating overnight at 30 °C and shaking at 240 rpm. Overnight cultures were then diluted 1000× in LB and incubated at 30 °C with shaking at 240 rpm until an optical density (OD) at 600 nm of ∼0.1 was reached, resulting in our starting culture. To achieve the desired pellicle testing geometry, we 3D printed culture molds (*i.e.*, volume-fixed containers) that have two rectangular compartments (25 mm × 7.5 mm × 10 mm deep) and one circular port for adding additional media to the mold after biofilm growth (Fig. S1). Rectangular sample geometries ease the calculation of mechanical properties and allow for comparisons across

conditions. Culture molds grow two pellicle strips from a connected media reservoir: one is used for tensile testing and the other for thickness measurements. The molds were secured within sterile magenta plant culture boxes and then filled with LBGM media (2% LB, 0.1 mM $MnCl_2$, and 3% glycerol) such that there was $\sim$1 cm of media covering the bottom of the culture (7.5–35 mL total volume). Our starting culture was inoculated into the molds, resulting in an $OD_{600} \approx 0.001$. The culture box was covered with parafilm and incubated at room temperature for 3 days prior to mechanical testing.

4.2 Biofilm harvesting and testing

After 3 days of growth, a scalpel was used to detach biofilm samples from the edges of the 3D printed molds. Biofilms were floated up out of their culture molds by adding additional media to the container (Movie S1 and Fig. S2). Then, one biofilm was transferred from the culture container to the TUTTUT bath. For metal ion studies, biofilm samples were floated in 50 mM $FeCl_3$, $FeCl_2$, $CuSO_4$, $CuCl$, $CaCl_2$, or $NaCl$ supplemented media for an exposure time of one hour prior to transferring to TUTTUT. The remaining biofilm was harvested on a glass slide for thickness measurements. Only biofilms in which both pellicle strips displayed a wrinkled morphology were used for measurements. Once in the TUTTUT bath, a clamp fabricated from rectangular coverglass slides (30 mm × 5 mm) with an $\sim$0.2 mm PDMS (1 : 10 cross-linker : silicone elastomer base) coating on one side was dropped onto one end of the biofilm and was secured into place on the bath using magnets. The free edge of the biofilm was then aligned with the extension piece of the cantilever, and the bath was raised to attach the sample to the cantilever grip, resulting in samples with aspect ratios (L/W) ranging from 1.8 to 3.9 (see the SI for all sample aspect ratios). To perform tensile testing, a linear actuator on TUTTUT caused the clamp to move away from the cantilever at a fixed velocity ($v_{actuator} = 0.1$ mm s^{-1}), stretching the biofilm at a fixed strain rate (0.00295–0.00446 s^{-1}) and causing the cantilever to deflect (Movie S1). Tensile tests in which the pellicle slipped from either the clamp or cantilever grip were excluded from analysis.

4.3 Thickness measurements

A Keyence VR-3000 3D Optical Profilometer (OP) was used to scan the 3D profiles of biofilms on glass slides. Using instrument analysis software, eight equally sized squares were selected within the sample, returning each square's average thickness with respect to the instrument stage. The thickness of the glass slide was subtracted from measurements, and the eight thickness values were averaged to obtain the average biofilm thickness for that culture container.

4.4 Investigation of pH effects

LBGM media (pH 7.0) were prepared as described in the Bacterial culture section and pH was adjusted to 2.0, 4.0, 8.0, or 10.0 using 1 M HCl and 1 M NaOH. To determine the impact of pH on the biofilm stress–strain response, biofilms were cultured for 3 days and then floated in pH adjusted media for an exposure time of one hour prior to tensile testing.

4.5 Chelation based analysis of biofilm-Fe^{3+} affinity

Pellicles were treated with 50 mM $FeCl_3$ for one hour prior to transfer to a wash bath, containing either 25 mM EDTA or LBGM media. After one hour, biofilms were transferred to TUTTUT for mechanical testing as described in the Biofilm harvesting and testing section.

4.6 Cantilever fabrication and calibration

Force readings were determined using the stiffness of cantilevers (S_c) fabricated from rectangular polyethylene terephthalate (PET) sheets. The cantilever material was selected to be at least 2× stiffer than biofilm samples. Cantilever calibrations and stress–strain calculations were performed as previously described.[37] In brief, S_c was calculated by measuring resonance frequency (f) at varying cantilever lengths (L_c). f was measured using a LK-G5000 Series Laser Displacement Sensor (1000 Hz) to capture the cantilever displacement (δ_{cant}) that occurred in response to tapping the cantilever. A Fourier transform was fit to these data to determine f. Three f measurements were taken for five different L_c values approximately 5 mm apart. We calculated the stiffness using f, L_c, total cantilever length (L_{total}), and total cantilever mass (m_{total}) by[67]

$$S_c = \frac{12\pi^2 f^2}{3.52^2} m_{total} \frac{L_c}{L_{total}} \qquad (1)$$

To establish a relationship between laser displacement (δ_{laser}) and δ_{cant}, a displacement is applied in the x-direction using the linear actuator and the resulting δ_{laser} is measured. A linear fit yields slope m_1. δ_{cant} is determined by dividing δ_{laser} by m_1, and force is then determined by $F = S_c \times \delta_{cant}$. Then, biofilm displacement (δ_{film}) is determined by $\delta_{film} = v_{actuator} \times t - \delta_{cant}$, where t is the time. Strain (ε) is determined by $\varepsilon = \frac{\delta_{film}}{L_0}$, where L_0 is the initial length of the film between grips. Stress (σ) is calculated by $\sigma = \frac{F}{w \times h}$, where w and h are the biofilm width and thickness, respectively.

4.7 Statistical analysis

All quantitative data are presented as mean ± standard deviation (SD) ($n \geq 3$). Statistical significance between sample means was determined using a one-way analysis of variance (ANOVA), followed by a Fisher's least significant difference (LSD) post hoc test for pairwise comparisons in OriginLab. Statistical significance with $p < 0.05$, $p < 0.01$, and $p < 0.001$ is indicated with an *, **, and ***, respectively.

Author contributions

Kiera J. Croland: conceptualization, data curation, formal analysis, investigation, methodology, validation, visualization, and writing—original draft. R. Kōnane Bay: conceptualization, funding acquisition, methodology, project administration,

resources, software, supervision, visualization, and writing---review and editing.

Conflicts of interest

There are no conflicts to declare.

Data availability

Supplementary information: all stress–strain responses and the properties extracted from stress–strain curves (low strain elastic moduli, maximum stresses, yield stresses, and failure strains). See DOI: https://doi.org/10.1039/d5sm01096a.

Acknowledgements

References

1 K. Kovach, M. Davis-Fields, Y. Irie, K. Jain, S. Doorwar, K. Vuong, N. Dhamani, K. Mohanty, A. Touhami and V. D. Gordon, *npj Biofilms Microbiomes*, 2017, **3**, 1.

2 D. G. Metcalf and P. G. Bowler, *Burns Trauma*, 2013, **1**, 2321–3868.

3 X. Li, L. Sun, P. Zhang and Y. Wang, *Coatings*, 2021, **11**, 294.

4 H. J. Busscher, H. C. van der Mei, G. Subbiahdoss, P. C. Jutte, J. J. A. M. van den Dungen, S. A. J. Zaat, M. J. Schultz and D. W. Grainger, *Sci. Transl. Med.*, 2012, **4**, 153rv10.

5 M. Cámara, W. Green, C. E. MacPhee, P. D. Rakowska, R. Raval, M. C. Richardson, J. Slater-Jefferies, K. Steventon and J. S. Webb, *npj Biofilms Microbiomes*, 2022, **8**, 1–8.

6 G. Liu, Y. Zhang, W.-J. Knibbe, C. Feng, W. Liu, G. Medema and W. van der Meer, *Water Res.*, 2017, **116**, 135–148.

7 P. S. Stewart and J. W. Costerton, *Lancet*, 2001, **358**, 135–138.

8 S. Saini, S. Tewari, J. Dwivedi and V. Sharma, *Mater. Adv.*, 2023, **4**, 1415–1443.

9 J. Huang, S. Liu, C. Zhang, X. Wang, J. Pu, F. Ba, S. Xue, H. Ye, T. Zhao, K. Li, Y. Wang, J. Zhang, L. Wang, C. Fan, T. K. Lu and C. Zhong, *Nat. Chem. Biol.*, 2019, **15**, 34–41.

10 L. M. González, N. Mukhitov and C. A. Voigt, *Nat. Chem. Biol.*, 2020, **16**, 126–133.

11 T. Guélon, J.-D. Mathias and P. Stoodley, in *Biofilm Highlights*, ed. H.-C. Flemming, J. Wingender and U. Szewzyk, Springer, Berlin, Heidelberg, 2011, pp. 111–139.

12 H. Boudarel, J.-D. Mathias, B. Blaysat and M. Grédiac, *npj Biofilms Microbiomes*, 2018, **4**, 17.

13 S. Grumbein, M. Opitz and O. Lieleg, *Metallomics*, 2014, **6**, 1441–1450.

14 M. Klotz, M. Kretschmer, A. Goetz, S. Ezendam, O. Lieleg and M. Opitz, *RSC Adv.*, 2019, **9**, 11521–11529.

15 E. N. Hayta and O. Lieleg, *Biomater. Sci.*, 2019, **7**, 4675–4686.

16 J. Yan, A. Moreau, S. Khodaparast, A. Perazzo, J. Feng, C. Fei, S. Mao, S. Mukherjee, A. Košmrlj, N. S. Wingreen, B. L. Bassler and H. A. Stone, *Adv. Mater.*, 2018, **30**, 1804153.

17 S. Liu, J. Huang, C. Zhang, L. Wang, C. Fan and C. Zhong, *Synth. Syst. Biotechnol.*, 2022, **7**, 965.

18 L. A. Bakhtiari, M. J. Wells and V. D. Gordon, *Biophys. Rev.*, 2021, **2**, 031402.

19 A. Sarlet, V. Ruffine, K. G. Blank and C. M. Bidan, *ACS Omega*, 2023, **8**, 4667–4676.

20 S. Grumbein, M. Werb, M. Opitz and O. Lieleg, *J. Rheol.*, 2016, **60**, 1085–1094.

21 I. Dogsa, M. Brloznik, D. Stopar and I. Mandic-Mulec, *PLoS One*, 2013, **8**, e62044.

22 E. C. Hollenbeck, C. Douarche, J.-M. Allain, P. Roger, C. Regeard, L. Cegelski, G. G. Fuller and E. Raspaud, *J. Phys. Chem. B*, 2016, **120**, 6080–6088.

23 M. Trejo, C. Douarche, V. Bailleux, C. Poulard, S. Mariot, C. Regeard and E. Raspaud, *Proc. Natl. Acad. Sci. U. S. A.*, 2013, **110**, 2011–2016.

24 C. Douarche, J.-M. Allain and E. Raspaud, *Biophys. J.*, 2015, **109**, 2195–2202.

25 M. U. Rahman, D. F. Fleming, L. Wang, K. P. Rumbaugh, V. D. Gordon and G. F. Christopher, *npj Biofilms Microbiomes*, 2022, **8**, 1–9.

26 I. B. Beech and J. Sunner, *Curr. Opin. Biotechnol*, 2004, **15**, 181–186.

27 J. A. Lemire, J. J. Harrison and R. J. Turner, *Nat. Rev. Microbiol.*, 2013, **11**, 371–384.

28 O. Lieleg, M. Caldara, R. Baumgärtel and K. Ribbeck, *Soft Matter*, 2011, **7**, 3307–3314.

29 C. Falcón García, M. Kretschmer, C. N. Lozano-Andrade, M. Schönleitner, A. Dragoŝ, Á. T. Kovács and O. Lieleg, *npj Biofilms Microbiomes*, 2020, **6**, 1.

30 H. Vlamakis, Y. Chai, P. Beauregard, R. Losick and R. Kolter, *Nat. Rev. Microbiol.*, 2013, **11**, 157–168.

31 S. S. Branda, F. Chu, D. B. Kearns, R. Losick and R. Kolter, *Mol. Microbiol.*, 2006, **59**, 1229–1238.

32 S. Gingichashvili, D. Duanis-Assaf, M. Shemesh, J. D. B. Featherstone, O. Feuerstein and D. Steinberg, *Microorganisms*, 2020, **8**, 62.

33 D. Romero, C. Aguilar, R. Losick and R. Kolter, *Proc. Natl. Acad. Sci. U. S. A.*, 2010, **107**, 2230–2234.

34 H. A. Hong, R. Khaneja, N. M. K. Tam, A. Cazzato, S. Tan, M. Urdaci, A. Brisson, A. Gasbarrini, I. Barnes and S. M. Cutting, *Res. Microbiol.*, 2009, **160**, 134–143.

35 M. Marzorati, P. Van den Abbeele, S. S. Bubeck, T. Bayne, K. Krishnan, A. Young, D. Mehta and A. DeSouza, *Microorganisms*, 2020, **8**, 1028.

36 A. Hashem, B. Tabassum and E. Fathi Abd_Allah, *Saudi J. Biol. Sci.*, 2019, **26**, 1291–1297.

37 R. K. Bay, S. Shimomura, Y. Liu, M. Ilton and A. J. Crosby, *Macromolecules*, 2018, **51**, 3647–3653.

38 Y. Liu, Y.-C. Chen, S. Hutchens, J. Lawrence, T. Emrick and A. J. Crosby, *Macromolecules*, 2015, **48**, 6534–6540.

39 W. J. Choi, R. K. Bay and A. J. Crosby, *Macromolecules*, 2019, **52**, 7489–7494.

40 R. K. Bay, K. Zarybnicka, J. Jančář and A. J. Crosby, *ACS Appl. Polym. Mater.*, 2020, **2**, 2220–2227.

41 R. K. Bay, T. Zhang, S. Shimomura, M. Ilton, K. Tanaka, R. A. Riggleman and A. J. Crosby, *Macromolecules*, 2022, **55**, 8505–8513.

42 H. Zhang, K. Fujiki, K. Ido, N. Kusayanagi, D. Sakagami, J. Li and Y. Okamura, *Polym. Test.*, 2020, **91**, 106825.

43 H. M. Thippeswamy, R. Shanbhog, M. N. Kumar, S. N. Prashanth and P. Smitha, *Sci. Rep.*, 2025, **15**, 10689.

44 H. S. Faust, *Am. J. Clin. Nutr.*, 1982, **35**, 1459–1467.

45 P. Vanysek, *CRC Hand Book of Chemistry and Physics*, 1993, pp. 5–92.

46 P. S. Stewart, *Biotechnol. Bioeng.*, 1998, **59**, 261–272.

47 V. Körstgens, H.-C. Flemming, J. Wingender and W. Borchard, *Water Sci. Technol.*, 2001, **43**, 49–57.

48 S. Geisel, E. Secchi and J. Vermant, *Interface Focus*, 2022, **12**, 20220032.

49 J. N. Wilking, T. E. Angelini, A. Seminara, M. P. Brenner and D. A. Weitz, *MRS Bull.*, 2011, **36**, 385–391.

50 I. W. Sutherland, *Microbiology*, 2001, **147**, 3–9.

51 J. Böhning, M. Ghrayeb, C. Pedebos, D. K. Abbas, S. Khalid, L. Chai and T. A. M. Bharat, *Nat. Commun.*, 2022, **13**, 7082.

52 E. Khare, N. Holten-Andersen and M. J. Buehler, *Nat. Rev. Mater.*, 2021, **6**, 421–436.

53 N. Ido, A. Lybman, S. Hayet, D. N. Azulay, M. Ghrayeb, S. Liddawieh and L. Chai, *Soft Matter*, 2020, **16**, 6180–6190.

54 S. Arnaouteli, N. C. Bamford, N. R. Stanley-Wall and Á. T. Kovács, *Nat. Rev. Microbiol.*, 2021, **19**, 600–614.

55 K. J. Henderson, T. C. Zhou, K. J. Otim and K. R. Shull, *Macromolecules*, 2010, **43**, 6193–6201.

56 M. Nishikawa and K. Kobayashi, *J. Bacteriol.*, 2021, **203**, 10–1128.

57 S. Aggarwal and R. M. Hozalski, *Biofouling*, 2010, **26**, 479–486.

58 D. N. Azulay, O. Spaeker, M. Ghrayeb, M. Wilsch-Bräuninger, E. Scoppola, M. Burghammer, I. Zizak, L. Bertinetti, Y. Politi and L. Chai, *Proc. Natl. Acad. Sci. U. S. A.*, 2022, **119**, e2118107119.

59 N. Jian, J. Wang, L. Zuo and K. Zhang, *Mater. Des.*, 2023, **225**, 111522.

60 H. Malektaj, A. D. Drozdov and J. deClaville Christiansen, *Polymers*, 2023, **15**, 3012.

61 A. Kovács, D. S. Nemcsok and T. Kocsis, *J. Mol. Struct. THEOCHEM*, 2010, **950**, 93–97.

62 R. M. Hutcheson, M. D. Engelmann and I. F. Cheng, *Biometals*, 2005, **18**, 43–51.

63 R. Cavaliere, J. L. Ball, L. Turnbull and C. B. Whitchurch, *MicrobiologyOpen*, 2014, **3**, 557–567.

64 X. Chen and P. S. Stewart, *Appl. Microbiol. Biotechnol.*, 2002, **59**, 718–720.

65 M. J. Tevethia and M. Mandel, *J. Bacteriol.*, 1970, **101**, 844–850.

66 M. Ghrayeb, S. Hayet, N. Lester-Zer, Y. Levi-Kalisman and L. Chai, *Microorganisms*, 2021, **9**, 529.

67 M. F. Ashby and D. Cebon, *J. Phys. IV France*, 1993, **03**, C7–C9.